View Article Online
DOI: 10.1039/D0TC00003E

Manipulation of Rashba effect in layered tellurides MTe (M=Ge, Sn, Pb)

Chang Liu[1], Heng Gao[1], Yongchang Li[1], Kangying Wang[1], Lee A. Burton[1], and Wei Ren[1,2,3,*]

1 Department of Physics, State Key Laboratory of Advanced Special Steel, and International Center of Quantum and Molecular Structures, Shanghai University, Shanghai 200444, China

2 Materials Genome Institute and Shanghai Key Laboratory of High Temperature Superconductors, Shanghai University, Shanghai 200444, China

3 State Key Laboratory of Solidification Processing, Northwestern Polytechnical University, Xi'an 710072, China

* renwei@shu.edu.cn

Abstract

Recently, trigonal layered GeTe was exfoliated from the rhombohedral germanium telluride using a sonication-assisted liquid-phase method in experiment. We identify the blue phosphorene-like MTe (M=Ge, Sn, and Pb) monolayers and bilayers as two-dimensional semiconductors with a large Rashba-type spin-orbit coupling effect that can be modulated by the external electric field. It is found that Rashba-type spin splitting occurs around the Γ point for both monolayer and bilayer MTe. For the bilayer MTe, we predict that the Rashba effect induced spin and momentum mismatch will give rise to a low recombination rate and long carrier lifetimes. We also obtain Rashba parameters and band gap values that are tunable with the perpendicular external electric field. In general, the low-dimensional MTe materials exhibit excellent functional characteristics, thus being promising for designing spin field-effect transistor and optoelectronics applications.

1. Introduction

Two-dimensional (2D) materials have received significant attention since graphene was successfully exfoliated from graphite in 2004.[1] Graphene has many interesting physical and chemical properties but unfortunately a zero energy band gap limits its practical applications. Thereafter, many alternative 2D materials were studied in experiment and theory, including but not limited to the hexagonal boron nitride (h-BN), transition metal dichalcogenides (TMDs), graphitic carbon nitride (g-C_3N_4), MXenes, phosphorene, silicone etc.[2-4] Recently, even freestanding $SrTiO_3$ and $BiFeO_3$ monolayers were synthesized by reactive molecular beam epitaxy.[5] It was found that tetragonal-like $BiFeO_3$ monolayers exhibit giant polarization with a large c/a value, together with other theoretical

View Article Online
DOI: 10.1039/D0TC00003E

prediction,[6-15] showing the possibility of novel phenomenon at the 2D limit. Mounet [16] and Singh [17] found hundreds of 2D compounds that could potentially be exfoliated from their parent three-dimensional (3D) materials based upon the high-throughput calculations. However, only a few structures have been synthesized and verified by experiments so far.[10, 12, 13]

Spin splitting of electronic energy band structures results from spin-orbit coupling (SOC) and an asymmetrical structure. Two types of spin splitting are mainly found in semiconductors, [18, 19] namely Rashba spin splitting and Dresselhaus spin splitting, which arise from the structure inversion asymmetry (SIA) and the bulk inversion asymmetry (BIA), respectively. Rashba spin splitting generally occurs due to the special inhomogeneity at the interface or surface, such as AlGaAs/GaAs,[20] which can be tuned by external electric fields and strains. Datta *et al.* proposed that Rashba effect could be used for controlling the spin precession in two-dimensional electron gas (2DEG).[21] Importantly, the Rashba effect can be manipulated by the external electric field, which offers an effective way to control the spin degree by gate voltage, in a so-called Datta-Das spin field effect transistor (FET). Since then, a great deal of research has been devoted to finding novel materials with large Rashba effect.[22-24] Recently, Rashba SOC induced indirect band gap and spin mismatch were used to explain the long carrier life time and diffusion length in the hybrid organic-inorganic perovskites, where the Rashba effect accounts for the outstanding photovoltaic performance. These results show the Rashba effect plays an important role in providing a means of all-electric-controlled spintronics and optoelectronics materials.

Conventional wisdom for search large Rashba spin splitting materials mainly focuses on strong SOC, *ie.* large atomic number elements, and inversion symmetry breaking, *ie.* interfaces or ferroelectric. Three-dimensional GeTe and SnTe are classified as ferroelectric Rashba semiconductors (FERSCs) with broken symmetry as well as strong spin-orbit interaction,[25-28] making them potential candidates for Datta-Das spin FET. Meanwhile, the Rashba semiconductors can be substantially doped without losing its ferroelectric properties, as confirmed in a recent theoretical report.[29] According to previous experimental works, [30-33] the Rashba effect is robust in ferroelectric GeTe and Mn-doped multiferroic $Ge_{1-x}Mn_xTe$, and the SOC band splitting can survive doping with magnetic Mn. Thus, doping is an efficient way to adjust Fermi level and make it practical to utilize the Rashba effect. However, with increasing demand of device miniaturization, ultra-thin 2D materials are attracting more attention. For instance, the giant Rashba semiconductor BiTeX (X=Cl, Br, I) was found to hold Rashba band splitting even in its monolayer form. [34] It will be interesting to further investigate large Rashba effect at the 2D limit.

In this letter, we focus on the buckled trigonal layered MTe (M=Ge, Sn, and Pb) as binary counterpart of blue phosphorus.[35-37] Recently, Zhang *et al.* reported that α-GeTe nanosheets could be exfoliated from ferroelectric bulk α-GeTe of the R3m space group.[38]

View Article Online
DOI: 10.1039/D0TC00003E

They demonstrated the existence of trigonal monolayer GeTe with an optical gap of 1.96 eV, which is larger than bulk phases due to the quantum confinement effect. Previously, several works reported that such buckled trigonal group-IV monochalcogenides possess isotropic piezoelectricity and promising photocatalytic properties.[35-37] Here, we perform density functional theory (DFT) computational analysis of the 2D group-IV tellurides MTe (M=Ge, Sn, and Pb). From our phonon spectra and formation energy calculations, it is found that MTe monolayers are both dynamically stable and thermodynamically stable. Furthermore, the low-dimensional MTe may also present sizable Rashba-type spin splitting, with Rashba parameters that are comparable with the bulk counterparts and can be regulated by external electric field. The bilayer MTe structures especially exhibit unique energy band structures that also indicate favorable properties for photovoltaics applications.

2. Computational model and methods

We use DFT with the projector augmented wave (PAW) as implemented in the Vienna ab initio simulation package (VASP).[39, 40] The electron exchange and correlation functional was treated by the generalized gradient approximation of Perdew-Burke-Ernzerhof (PBE).[40] The weak van der Waals interaction was described by the optB86b-vdW functional.[41, 42] The energy cutoff was 550 eV and the k-point grid sampling grid was generated using the gamma point centered scheme with 21 × 21× 1 points. The energy convergence was set to 10^{-8} eV and the maximum force on each atom was less than 10^{-3} eV/Å in relaxation and self-consistent calculations. We use Gaussian smearing method with a width of 0.02 eV. A vacuum slab of 20 Å in the c-direction was added to avoid periodic interactions. Phonon dispersion analysis was performed with a 4 × 4 × 1 supercell by using the PHONOPY code.[43-45]

3. Results and Discussions

3.1 The geometrical structure and stability of monolayer MTe

The optimized structure of MTe bulk, monolayer and bilayer structures are shown in Figure 1. The bulk structure consists of stacked 2D trigonal layers containing M and Te atoms in two parallel planes. It appears as an isotropic honeycomb from top view and a puckered configuration from the side view, which is analogous to the blue phosphorus. We use a variety of different functionals and vdW corrections to calculate the physical properties, which are shown in Table 1. The optimized lattice parameters of GeTe, SnTe and PbTe monolayer are 3.96 Å, 4.18 Å and 4.26 Å, respectively. The buckle height and band gap of GeTe monolayer are 1.59 Å with optB86b-vdW corrections and 1.88 eV by

View Article Online
DOI: 10.1039/D0TC00003E

using HSE06 with SOC, in good agreement with experiment and other reports.[40,43]

Structures	Monolayer			Bilayer		
MTe (M=Ge, Sn, Pb)	GeTe	SnTe	PbTe	GeTe	SnTe	PbTe
Lattice parameter a (Å)	3.96	4.18	4.26	4.03	4.26	4.36
Bond length l (Å)	2.75	2.93	3.00	2.76	2.95	3.03
Buckling height h (Å)	1.59	1.71	1.73	5.37	5.82	5.96
optB86b-vdW+SOC Band gap E_g (eV)	1.46	1.51	1.19	0.33	0.40	0
HSE06+SOC Band gap E_g (eV)	1.88	1.86	1.60	0.46	0.53	0.26
Rashba energy ΔE_C (meV)	5.91	5.71	2.09	13.0	13.0	13.1
Rashba energy ΔE_V (meV)				7.94	7.95	7.93
Rashba parameter α_R^C (eVÅ)	0.60	0.62	0.60	1.10	1.02	1.05
Rashba parameter α_R^V (eVÅ)				1.35	0.79	0.45

Table. 1. Structural parameters, band gaps, Rashba energies and Rashba parameters of MTe monolayer and bilayer.

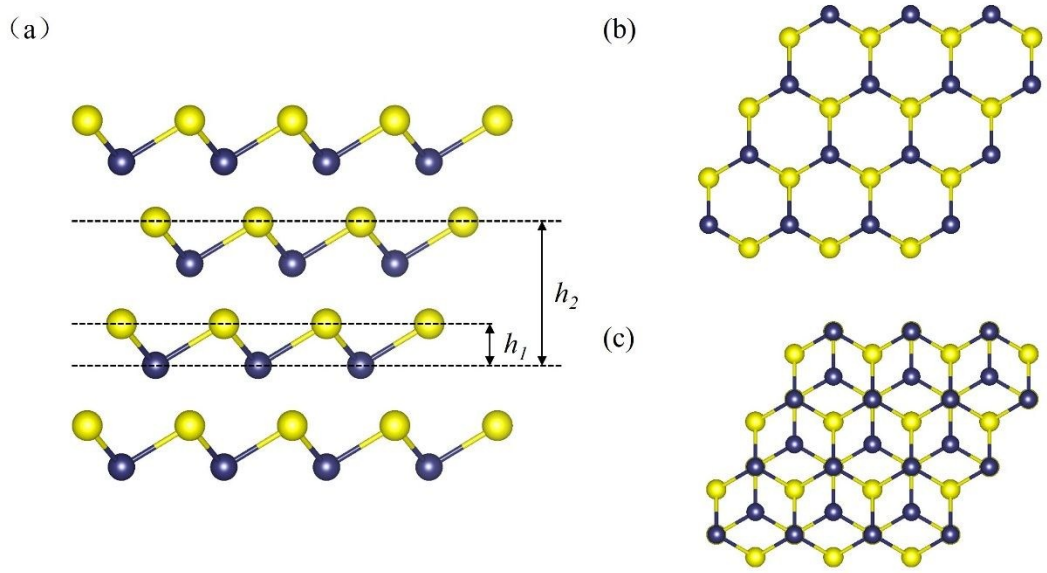

Figure.1. (a) The optimized structure of bulk MTe (M=Ge, Sn, Pb). The lattice of bulk MTe is represented by solid lines. The monolayer and bilayer MTe structures are framed with dashed lines. Top views of (b) monolayer and (c) bilayer (AC stacking). M and Te atoms are shown in gray and yellow colors, respectively.

To confirm dynamical stabilities of the monolayer MTe, we performed phonon dispersion calculations as shown in the Supplementary Information Figure S1. From the

View Article Online
DOI: 10.1039/D0TC00003E

phonon spectra, we confirm that all structures are kinetically stable based on the absence of significant imaginary frequency throughout the Brillouin zone.[46] To further investigate the thermodynamic stability of the three monolayers, we calculated the formation energies for MTe monolayer. We define the formation energy as $E_b = (nE_M + nE_{Te} - E_{(MTe)n})/n$ where E_M,E_{Te} , $E_{(MTe)n}$ are the total energies of a single M atom, Te atom, and MTe monolayer respectively, and n is the number of formula units. The formation energies of GeTe, SnTe, and PbTe are found to be 8.23 eV, 7.26 eV, and 7.11 eV, respectively. These results indicate that all three structures are stable and GeTe monolayer is the most stable among these three structures.

3.2 Electronic properties of monolayer MTe.

To investigate the electronic properties of group-IV tellurides, we have calculated their band structures, which are presented in Figure 2(a)-(f). In Table 1, we note that all three tellurides are semiconductors at the level of optB86b-vdW with SOC and HSE06 with SOC. GeTe and SnTe monolayers have indirect band gaps of 1.88 eV and 1.86 eV, as the valence band maximum (VBM) and conduction band minimum (CBM) are located at Γ point and a point between M- Γ line in the first Brillouin zone, respectively. However, PbTe monolayer is a direct band gap semiconductor with a smaller band gap of 1.60 eV with both VBM and CBM at Γ point.

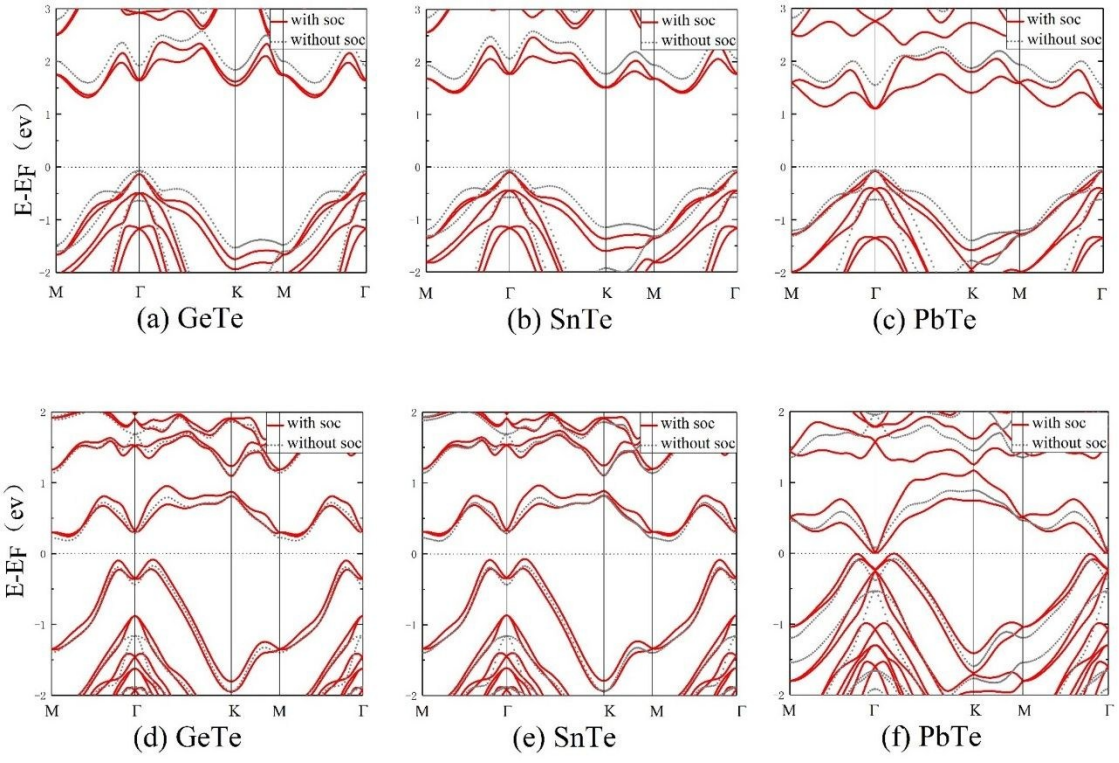

Figure.2. Band structures of MTe (a)-(c) monolayer and (d)-(f) bilayer by using optB86b-vdW with and without SOC.

View Article Online
DOI: 10.1039/D0TC00003E

We consider carefully the SOC effect in these systems, because of the heavy elements in the trigonal lattices. In general, the CBM are down-shifted with SOC, so that band gap becomes smaller for all systems and the inclusion of SOC removes band degeneracy from C_{3v} symmetry. As shown in Figure 3, it is interesting that the conduction band shows a sizable Rashba splitting at the Γ point due to out-of-plane broken symmetry. GeTe, SnTe and PbTe monolayers have similar Rashba spin splitting around Γ point but with different amplitudes. The Rashba SOC can be expressed as $H_R = \alpha_R(k_x\sigma_y - k_y\sigma_x)$, thus the energy dispersion relation should be modified as $E(k) = \frac{\hbar^2\vec{k}^2}{2m} + \alpha_R|\Delta k|$.

To further understand the Rashba splitting, we have calculated the spin texture of the conduction band maximum at Γ point. In Figure 3(b), we use the black arrows in-plane to represent the S_x and S_y vector components and the color for the out-of-plane S_z component. We see clearly that the spin arrows show anticlockwise rotation pattern for the outer band, and clockwise for inner band, which visually verify the physical characteristic of the Rashba splitting. We can further measure the Rashba effect through calculating the Rashba energy E_R, the k-space shift K_R and the Rashba parameter α_R by numerical fitting the DFT calculations. In nearly-free-electron approximation, the Rashba parameter is defined as $\alpha_R = 2E_R/K_R$. Thus our calculated $\alpha_R$values are 0.60 eVÅ, 0.62 eVÅ and 0.60 eVÅ for GeTe, SnTe and PbTe respectively at the optB86b-vdW level. These values are comparable to other 2D Rashba materials, such as the Au (111) surface,[47] Janus TMD monolayers[48] and the InGaAs/InAlAs interface.[49] It is worth mentioning that GeTe and SnTe bulk counterparts also possess giant Rashba splitting at the Z point because of the three-fold rotation symmetry.[27]

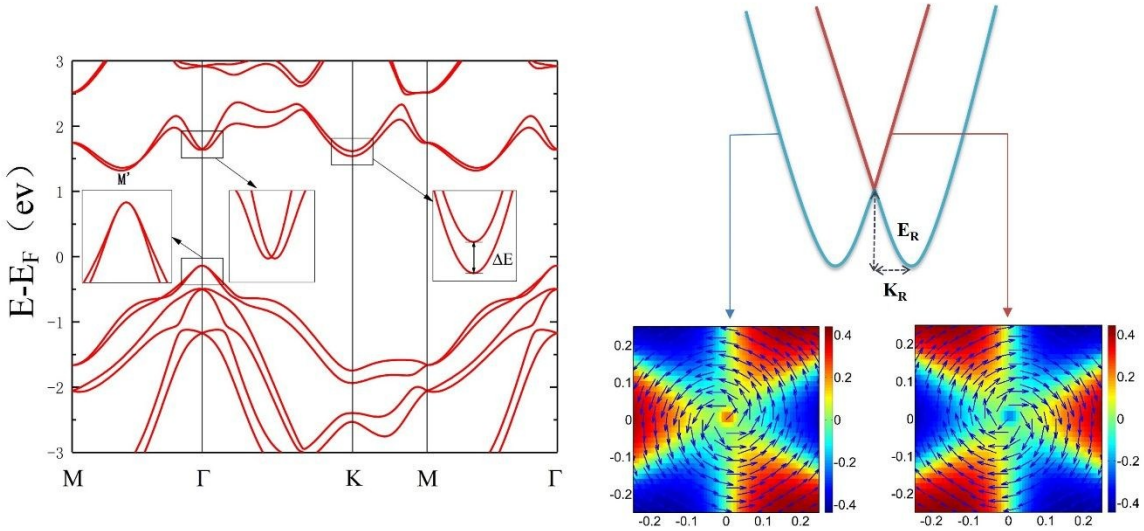

(a) (b)

View Article Online
DOI: 10.1039/D0TC00003E

Figure.3. (a) The band structure of GeTe monolayer with SOC. (b) Spin textures of the CBM around the Γ point, where the inner band is red and the outer band is blue.

Ferroelectric bulk phases MTe (M=Ge, Sn) have been confirmed as good candidate materials to control the direction of electronic spin polarization,[25-28, 50, 51] here we consider the polarization and its effects in the low-dimensional MTe. The estimated polarization of group IV monochalcogenides is about 2-3 $\times 10^{-11}$ C/m, while the monolayer SnTe has the largest value of 3×10^{-11}C/m. These quantities are one order of magnitude larger than III-V binary AB monolayers due to the larger electronegativity in our IV-VI systems.[52] The Born effective charge Z^* is useful for confirming the polarization values and also estimating the depolarization filed. We calculate the zz component of the charge tensor to be Z^*_{zz} ~ 0.1e, which suggests a weak depolarization field. Previous experiment and simulations also showed that surface defects and cation vacancies might enhance the polarization effect and weaken the depolarization field in the GeTe film.[53] According to the literature, the amplitude of Rashba splitting can be tuned by the polarization, buckle height and SOC strength of different elements.[48, 54-56] In the case of monolayer GeTe, we set and tested three different buckle heights: namely 1.56 Å, 2.45Å and 2.64Å, with the corresponding calculated α_R as 0.68eVÅ, 1.12 eVÅ and 1.37 eVÅ, respectively. Furthermore, we fixed the buckle height (h) with same value of 2.45 Å, and then found the calculated Rashba parameters to 1.39 eVÅ, 1.41 eVÅ and 1.46 eVÅ for GeTe, SnTe and PbTe respectively. The Rashba parameters α_R of PbTe is the largest because of its most significant SOC effect. These results agree well with previously reported work.[48, 55-57] We also find a twofold degeneracy at Γ point and a giant valley spin splitting at K points due to lack mirror symmetry, as shown in the figure 3(a), which is similar with GaAs monolayer.[54, 58] It is shown from figure 3(a) that a band gap (ΔE=191meV) opens due to the strong Zeeman-like magnetic field at K point. Such valley spin splitting also holds for –K point.

3.3 The geometrical structures and electronic properties of bilayer MTe

For bilayer MTe, we consider four different stacking orders: namely AA, AB, AB-1, and AC. In the case of bilayer GeTe, the energy comparison indicates that the most stable type is AC stacking, as that in the bulk configuration. In fact, we find the AC bilayer stacking to be the lowest energy for all three MTe systems. Bilayer MTe lattice parameters and band gaps are listed in Table 1. As shown in Figure 1, AC stacking bilayer MTe also breaks the symmetry along the out-of-plane direction, as does the polarization of the monolayer.

After geometry optimization, we calculated the electronic structures of bilayer MTe. In Table 1 and Figure S2(d)-(f), they are all small indirect gap semiconductors at the HSE level, except that the bilayer PbTe appears to be metallic at the optB86b-vdW level. When including SOC, we see that the band gap becomes smaller because the conduction bands shift down compared to the results without SOC. The bilayer structural inversion

View Article Online
DOI: 10.1039/D0TC00003E

asymmetry removes spin degeneracy and leads to Rashba splitting for both conduction and valence bands. However, for monolayers, only the conduction band shows Rashba splitting around Γ point. This indicates that the symmetry character for the VBM and the CBM is same for bilayer systems contrast with the monolayers. The calculated conduction band Rashba parameters α_R^C is 1.10 eV Å, 1.02 eV Å and 1.05 eV Å for bilayer GeTe, SnTe and PbTe respectively, which are twice as large as monolayer parameters because of doubled dipole moment. The corresponding Rashba parameters α_R^V at the valence bands are 1.35 eV Å, 0.79 eV Å and 0.45 eV Å, respectively. In 2D system, it is unusual that valence and conduction bands both exhibit Rashba splitting and in this case it could be interpreted as arising from a combination of strong SOC and narrow band gap.

Importantly, we propose that as the consequence of Rashba effect, a spin and momentum mismatch may induce low-radiative recombination rate and long carrier lifetime in bilayer MTe as illustrated in Figure 4(a). Taking bilayer GeTe as an example, the strong SOC and out-of-plane broken symmetry split the twofold degenerate bands into bands with opposite spin orientations (clockwise and anticlockwise). As a result, based on spin textures of VBM1 and CBM1, a direct optical transition is forbidden while indirect optical transition is allowed form CBM1 to VBM2 for the consistent spin states. Thus the intrinsic indirect band gap induced momentum mismatch further suppresses the recombination process, which is different from it bulk's spin texture at VBM and CBM.[25, 27] As a matter of fact, Zheng *et al*.[59] proposed the same mechanism to explain the long carrier life time and diffusion length in the hybrid organic-inorganic perovskites, where the Rashba effect accounts for the outstanding photovoltaic performance. The presence of strong SOC and bulk ferroelectricity in such 3D Rashba materials has been shown to be an intrinsic mechanism for the enhancement of optoelectronic applications, including the high incident photon-to-electron conversion efficiency.[60-63] So we believe that similar effect was found in bilayer MTe and would also provide possibility for 2D photovoltaic and optoelectronic applications. Furthermore, Ji *et al.* considered multilayer Ge-based IV-VI compounds provide great separation of electrons and holes for photocatalysts because of its intrinsic dipole and suitable band gap.[36] Such consequences of spin-forbidden process could be observed by experiment and make bilayer MTe attractive in light harvesting applications.

View Article Online
DOI: 10.1039/D0TC00003E

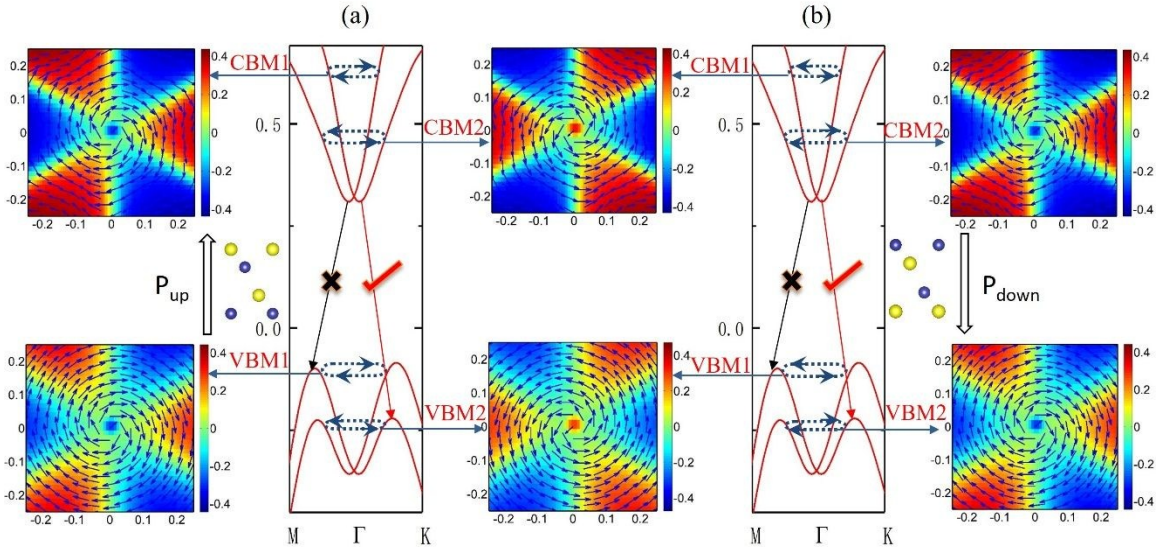

Figure.4. (a) Band structure of GeTe bilayer with SOC and spin texture of the CBM around the Γ point. (b) Band structures and spin textures for opposite polarizations of GeTe bilayer. Black cross denotes direct optical transition is forbidden, while for red tick indirect optical transition is allowed.

Furthermore, previous literature[50, 53] mentioned that 3 to 5 nm thick GeTe films could retain ferroelectric properties, so we set up the opposite atomic arrangements for reversed polarization as shown in the Figure 4(b). Switching the polarization direction leads to complete reversal of Rashba spin texture at CBM and VBM, but without affecting the whole band dispersion, as a characteristic of FERSCs. To visualize the spin texture, we use the vector arrows and background colors to represent the electron spin states in the reciprocal space. Based on the electric field control of polarization inversion, we can design spintronic devices with a manipulation mechanism of the electron spins from band theory.

3.4 Electric field control Rashba effect and Band gaps

To probe the effect of electric field on Rashba ferroelectric semiconductors, we applied the external electric field to the MTe monolayers perpendicular to the 2D plane, which has an equivalent effect on the band structure as adjusting the buckle height. The positive external electric field points from M to Te, which is in line with a local electric dipole moment. Previous studies have shown that the strength of Rashba splitting is tunable by external electric field, so it is also expected for these MTe systems.[23-24, 53, 60] From Figure 5(a), the external electric field can modulate band gaps and Rashba splitting parameters. Generally the Rashba parameters increase with the external electric field, and a negative field suppresses the Rashba splitting parameters. The PbTe monolayer reaches the largest Rashba parameter of about 0.91 eVÅ under the positive external electric field of 0.5 eV/Å.

View Article Online
DOI: 10.1039/D0TC00003E

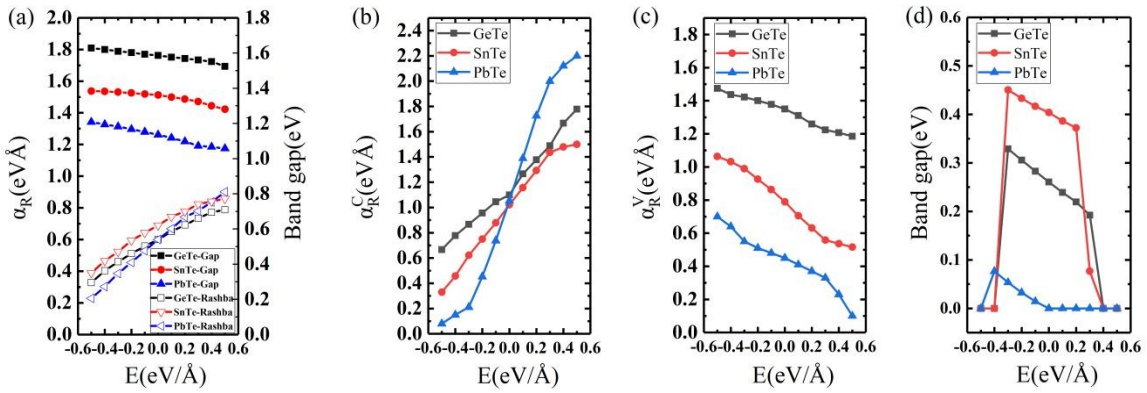

Figure 5. (a) Calculated Rashba parameters and band gaps at the optB86b-vdW level as function of external electric field for MTe monolayers. Calculated Rashba parameters at (b) CBM and (c) VBM as function of external electric field for MTe bilayers. (d) Band gaps of MTe bilayers as function of external electric field.

The band gap of the MTe monolayer is also dependent on the external electric field, as well as the Rashba splitting. Among the three systems, we find that band gap and Rashba splitting of the PbTe monolayer is most sensitive to the external electric field, with an indirect band gap ranging from 1.21 eV (under -0.5 eV/Å) to 1.06 eV (under 0.5 eV/Å). Furthermore, we calculated the electric field effect on the bilayer MTe compounds as shown in Figure 5 (b)-(d). The positive electric field direction is again parallel to the direction of the intrinsic polarization of bilayer MTe. As shown in Figure 5(b), the Rashba parameter α_R^C at conduction band minima displays approximately linear response to electric field, suggesting that a positive electric field increases the Rashba band splitting while a negative electric field decreases α_R^C. This effect is similar to the single layer configuration in Figure 5(a). However, for the valence band, the Rashba parameter α_R^V is suppressed by positive electric field and enhanced by negative electric field, in contrast with the CBM case. A more detailed analysis shows that bilayer PbTe strongly responds to the external electric field, with the Rashba parameter α_R^V ranging from 0 to 2.23 eV Å. The maximal values of Rashba parameters are 1.49 eV Å, 1.77 eV Å and 2.23 eV Å for GeTe, SnTe and PbTe respectively.

Finally, we look at the band gap behavior versus the electric field strength, and find that the MTe monolayers have robust band gaps above 1 eV. On the other hand, under large external electric field, MTe bilayers tend to become metallic which is due to the nearly free electron (NFE) states.[64] As shown in Figure S3, these NFE bands (black curves) are contributed by electrons (color bands) located outside of M or Te atoms, and they exhibit parabolic energy dispersions with respect to the crystal wave vector. However, for both bilayers and monolayers, the band gap reductions have a linear response to the applied field. As mentioned above, an external electric field regulation of electron spin is even more attractive than a magnetic field effect for the 2D materials. This functionality could be

View Article Online
DOI: 10.1039/D0TC00003E

utilized for electronic device applications, such as spintronic field effect transistor (FET).

Under the increasing trend of microelectronic device miniaturization, we propose to construct the 2D MTe spin-FET. The stability of the ferroelectric phase in such ultrathin films of Rashba semiconductors may lead excellent performance in low-dimensional spintronics and optoelectronics. Moreover, there will also be potential applications when they are integrated with magnetic systems or phase-change materials. A novel class of multifunctional heterostructure devices with high density non-volatility and field-tunable effects are awaited for further technological investigations.[21]

4. Conclusions

In this work, we systematically investigate and reveal the Rashba spin splitting of two-dimensional blue phosphorene-like MTe (M=Ge, Sn and Pb), for both monolayer and bilayer configurations. In the case of single layer MTe, Rashba effect and valley spin splitting occur in the conduction band at Γ point and K point respectively due to the breaking of inversion and mirror symmetry. A sizable Rashba effect is also found in bilayer MTe around Γ point and the polarization reversal can switch the spin texture characteristics. Within this framework, the momentum mismatch for opposite spin helicities at VBM and CBM could enhance the carrier lifetimes and decrease radiative recombination coefficients for photonic devices. Furthermore, an external electric field is shown to modulate the Rashba effect and band gap values for both monolayer and bilayer MTe. These findings demonstrate that group-IV monochalcogenides materials are promising for spintronics and optoelectronic properties.

5. Acknowledgements

This work was supported by the National Natural Science Foundation of China (Grant No. 51672171, 51861145315 and 51911530124), Shanghai Municipal Science and Technology Commission Program (No.19010500500), State Key Laboratory of Solidification Processing in NWPU (SKLSP201703), Austrian Research Promotion Agency (FFG, Grant No. 870024, project acronym MagnifiSens), and Independent Research Project of State Key Laboratory of Advanced Special Steel and Shanghai Key Laboratory of Advanced Ferrometallurgy at Shanghai University.

6. References

1. K. S. Novoselov, A. K. Geim, S. V. Morozov, D. Jiang, Y. Zhang, S. V. Dubonos, I. V. Grigorieva and A. A. Firsov, *Science*, 2004, **306**, 666-669.
2. L. C. Gomes and A. Carvalho, *Physical Review B*, 2015, **92**, 085406.
3. B. Radisavljevic, A. Radenovic, J. Brivio, V. Giacometti and A. Kis, *Nat Nanotechnol*, 2011, **6**, 147-150.
4. R. Ganatra and Q. Zhang, *ACS Nano*, 2014, **8**, 4074-4099.
5. D. Ji, S. Cai, T. R. Paudel, H. Sun, C. Zhang, L. Han, Y. Wei, Y. Zang, M. Gu, Y. Zhang, W. Gao, H. Huyan, W. Guo, D. Wu, Z. Gu, E. Y. Tsymbal, P. Wang, Y. Nie and X. Pan, *Nature*, 2019, **570**, 87-90.

View Article Online
DOI: 10.1039/D0TC00003E

6. K. T. Kang, C. J. Roh, J. Lim, T. Min, J. H. Lee, K. Lee, T. Y. Lee, S. Kang, D. Seol, J. Kim, H. Ohta, A. Khare, S. Park, Y. Kim, S. C. Chae, Y. S. Oh, J. Lee, J. Yu, J. S. Lee and W. S. Choi, *Adv Mater*, 2019, **31**, e1808104.
7. M. Wu and P. Jena, *Wiley Interdisciplinary Reviews: Computational Molecular Science*, 2018, **8**, e1365.
8. B. Xu, H. Xiang, Y. Xia, K. Jiang, X. Wan, J. He, J. Yin and Z. Liu, *Nanoscale*, 2017, **9**, 8427-8434.
9. M. Wu and X. C. Zeng, *Nano Lett*, 2017, **17**, 6309-6314.
10. W. Ding, J. Zhu, Z. Wang, Y. Gao, D. Xiao, Y. Gu, Z. Zhang and W. Zhu, *Nat Commun*, 2017, **8**, 14956.
11. A. Chandrasekaran, A. Mishra and A. K. Singh, *Nano Letters*, 2017, **17**, 3290-3296.
12. F. Liu, L. You, K. L. Seyler, X. Li, P. Yu, J. Lin, X. Wang, J. Zhou, H. Wang, H. He, S. T. Pantelides, W. Zhou, P. Sharma, X. Xu, P. M. Ajayan, J. Wang and Z. Liu, *Nat Commun*, 2016, **7**, 12357.
13. K. Chang, J. Liu, H. Lin, N. Wang, K. Zhao, A. Zhang, F. Jin, Y. Zhong, X. Hu, W. Duan, Q. Zhang, L. Fu, Q.-K. Xue, X. Chen and S.-H. Ji, *Science*, 2016, **353**, 274.
14. X. Liu, Y. Yang, T. Hu, G. Zhao, C. Chen and W. Ren, *Nanoscale*, 2019, **11**, 18575-18581.
15. C. Liu, T. Hu, Y. Wu, H. Gao, Y. Yang and W. Ren, *J Phys Condens Matter*, 2019, **31**, 235702.
16. N. Mounet, M. Gibertini, P. Schwaller, D. Campi, A. Merkys, A. Marrazzo, T. Sohier, I. E. Castelli, A. Cepellotti, G. Pizzi and N. Marzari, *Nat Nanotechnol*, 2018, **13**, 246-252.
17. A. K. Singh, B. C. Revard, R. Ramanathan, M. Ashton, F. Tavazza and R. G. Hennig, *Physical Review B*, 2017, **95**, 155426.
18. Y. A. Bychkov and E. I. Rashba, *Journal of physics C: Solid state physics*, 1984, **17**, 6039.
19. G. Dresselhaus, *Physical Review*, 1955, **100**, 580.
20. D. Stein, K. v. Klitzing and G. Weimann, *Physical review letters*, 1983, **51**, 130.
21. S. Datta and B. Das, *Applied Physics Letters*, 1990, **56**, 665-667.
22. K. Li, X. Xian, J. Wang and N. Yu, *Applied Surface Science*, 2019, **471**, 18-22.
23. Y.-H. Meng, W. Bai, H. Gao, S.-J. Gong, J.-Q. Wang, C.-G. Duan and J.-H. Chu, *Nanoscale*, 2017, **9**, 17957-17962.
24. S.-J. Gong, C.-G. Duan, Y. Zhu, Z.-Q. Zhu and J.-H. Chu, *Physical Review B*, 2013, **87**, 035403.
25. F. Zheng, L. Z. Tan, S. Liu and A. M. Rappe, *Nano letters*, 2015, **15**, 7794-7800.
26. C. W. Myung, S. Javaid, K. S. Kim and G. Lee, *ACS Energy Letters*, 2018, **3**, 1294-1300.
27. X. Zhang, J.-X. Shen, W. Wang and C. G. Van de Walle, *ACS Energy Letters*, 2018, **3**, 2329-2334.
28. Z.-G. Yu, *The journal of physical chemistry letters*, 2016, **7**, 3078-3083.
29. X. Zhang, J.-X. Shen and C. G. Van de Walle, *The journal of physical chemistry letters*, 2018, **9**, 2903-2908.
21. S. Picozzi, *Frontiers in Physics*, 2014, **2**, 10.
31. M. Liebmann, C. Rinaldi, D. Di Sante, J. Kellner, C. Pauly, R. N. Wang, J. E. Boschker, A. Giussani, S. Bertoli, M. Cantoni, L. Baldrati, M. Asa, I. Vobornik, G. Panaccione, D. Marchenko, J. Sanchez-Barriga, O. Rader, R. Calarco, S. Picozzi, R. Bertacco and M. Morgenstern, *Adv Mater*, 2016, **28**, 560-565.
32. D. Di Sante, P. Barone, R. Bertacco and S. Picozzi, *Adv Mater*, 2013, **25**, 509-513.
33. E. Plekhanov, P. Barone, D. Di Sante and S. Picozzi, *Physical Review B*, 2014, **90**, 161108.
34. H. Djani, A. C. Garcia-Castro, W.-Y. Tong, P. Barone, E. Bousquet, S. Picozzi and P. Ghosez, *npj Quantum Materials*, 2019, **4**, 51.
35. H. J. Elmers, R. Wallauer, M. Liebmann, J. Kellner, M. Morgenstern, R. N. Wang, J. E. Boschker, R. Calarco, J. Sánchez-Barriga, O. Rader, D. Kutnyakhov, S. V. Chernov, K. Medjanik, C. Tusche, M. Ellguth, H. Volfova, S. Borek, J. Braun, J. Minár, H. Ebert and G. Schönhense, *Physical Review B*, 2016, **94**, 201403.
36. J. Krempasky, S. Muff, F. Bisti, M. Fanciulli, H. Volfova, A. P. Weber, N. Pilet, P. Warnicke, H. Ebert, J. Braun, F. Bertran, V. V. Volobuev, J. Minar, G. Springholz, J. H. Dil and V. N. Strocov, *Nat Commun*, 2016, **7**, 13071.
37. J. Krempaský, S. Muff, J. Minár, N. Pilet, M. Fanciulli, A. P. Weber, E. B. Guedes, M. Caputo, E. Müller, V. V. Volobuev, M. Gmitra, C. A. F. Vaz, V. Scagnoli, G. Springholz and J. H. Dil, *Physical Review X*, 2018, **8**, 021067.
38. J. Krempaský, H. Volfová, S. Muff, N. Pilet, G. Landolt, M. Radović, M. Shi, D. Kriegner, V. Holý, J. Braun, H. Ebert, F. Bisti, V. A. Rogalev, V. N. Strocov, G. Springholz, J. Minár and J. H. Dil, *Physical Review B*, 2016, **94**, 205111.
39. Y. Ma, Y. Dai, W. Wei, X. Li and B. Huang, *Phys Chem Chem Phys*, 2014, **16**, 17603-17609.
40. M. Qiao, Y. Chen, Y. Wang and Y. Li, *Journal of Materials Chemistry A*, 2018, **6**, 4119-4125.
41. Y. Ji, M. Yang, H. Dong, T. Hou, L. Wang and Y. Li, *Nanoscale*, 2017, **9**, 8608-8615.

View Article Online
DOI: 10.1039/D0TC00003E

42. T. Hu and J. Dong, *Phys Chem Chem Phys*, 2016, **18**, 32514-32520.
43. P. Zhang, F. Zhao, P. Long, Y. Wang, Y. Yue, X. Liu, Y. Feng, R. Li, W. Hu and Y. Li, *Nanoscale*, 2018, **10**, 15989-15997.
44. P. E. Blöchl, *Physical Review B*, 1994, **50**, 17953-17979.
45. G. Kresse and J. Furthmüller, *Computational Materials Science*, 1996, **6**, 15-50.
46. J. Klimeš, D. R. Bowler and A. Michaelides, *Physical Review B*, 2011, **83**, 195131.
47. J. Klimes, D. R. Bowler and A. Michaelides, *J Phys Condens Matter*, 2010, **22**, 022201.
48. A. Togo, F. Oba and I. Tanaka, *Physical Review B*, 2008, **78**, 134106.
49. A. Togo and I. Tanaka, *Scripta Materialia*, 2015, **108**, 1-5.
50. S. Baroni, S. de Gironcoli, A. Dal Corso and P. Giannozzi, *Reviews of Modern Physics*, 2001, **73**, 515-562.
51. H. Zheng, X.-B. Li, N.-K. Chen, S.-Y. Xie, W. Q. Tian, Y. Chen, H. Xia, S. B. Zhang and H.-B. Sun, *Physical Review B*, 2015, **92**, 115307.
52. S. LaShell, B. A. McDougall and E. Jensen, *Physical Review Letters*, 1996, **77**, 3419-3422.
53. T. Hu, F. Jia, G. Zhao, J. Wu, A. Stroppa and W. Ren, *Physical Review B*, 2018, **97**, 235404.
54. J. Nitta, T. Akazaki, H. Takayanagi and T. Enoki, *Physical Review Letters*, 1997, **78**, 1335-1338.
55. A. V. Kolobov, D. J. Kim, A. Giussani, P. Fons, J. Tominaga, R. Calarco and A. Gruverman, *APL Materials*, 2014, **2**, 066101.
56. C. Rinaldi, S. Varotto, M. Asa, J. Slawinska, J. Fujii, G. Vinai, S. Cecchi, D. Di Sante, R. Calarco, I. Vobornik, G. Panaccione, S. Picozzi and R. Bertacco, *Nano Lett*, 2018, **18**, 2751-2758.
57. D. Di Sante, A. Stroppa, P. Barone, M.-H. Whangbo and S. Picozzi, *Physical Review B*, 2015, **91**, 195402.
58. X. Wang, L. Zhou, J. Feng, S. Wang, H. Qian, H. Tong and X. Miao, *Applied Physics Letters*, 2018, **113**, 232903.
59. J. Wu, Y. Yang, H. Gao, Y. Qi, J. Zhang, Z. Qiao and W. Ren, *AIP Advances*, 2017, **7**, 035218.
60. Q.-F. Yao, J. Cai, W.-Y. Tong, S.-J. Gong, J.-Q. Wang, X. Wan, C.-G. Duan and J. H. Chu, *Physical Review B*, 2017, **95**, 165401.
61. P. Z. Hanakata, A. S. Rodin, A. Carvalho, H. S. Park, D. K. Campbell and A. H. Castro Neto, *Physical Review B*, 2017, **96**, 161401.
62. E. Bruyer, D. Di Sante, P. Barone, A. Stroppa, M.-H. Whangbo and S. Picozzi, *Physical Review B*, 2016, **94**, 195402.
63. S. Saberi-Pouya, T. Vazifehshenas, T. Salavati-fard, M. Farmanbar and F. M. Peeters, *Physical Review B*, 2017, **96**, 075411.
64. M. Khazaei, A. Ranjbar, M. Ghorbani-Asl, M. Arai, T. Sasaki, Y. Liang and S. Yunoki, *Physical Review B*, 2016, **93**, 205125.

View Article Online
DOI: 10.1039/D0TC00003E

A table of contents entry

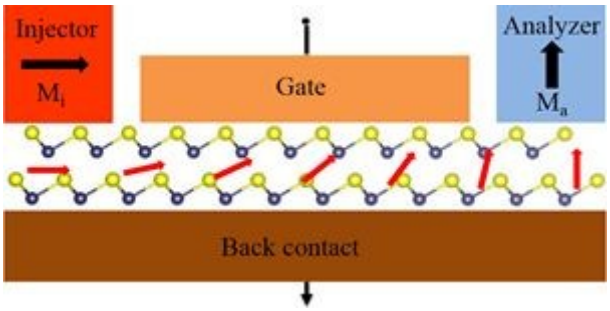

Designing an electric-field controlled Rashba spin FET on two-dimensional GeTe